Tunable Near-Infrared Localized Surface Plasmon Resonances of Djurleite Nanocrystals: Effects of Size, Shape, Surface-ligands and Oxygen Exposure Time

ARTICLE · MAY 2015

DOI: 10.1039/C5TC01310K

6 AUTHORS, INCLUDING:

Dongxu Zhu
Beijing Jiaotong University
2 PUBLICATIONS **1** CITATION
SEE PROFILE

Aiwei Tang
Beijing Jiaotong University
81 PUBLICATIONS **808** CITATIONS
SEE PROFILE

Miao Wang
Beijing Jiaotong University
7 PUBLICATIONS **23** CITATIONS
SEE PROFILE

Feng Teng
Beijing Jiaotong University
224 PUBLICATIONS **1,519** CITATIONS
SEE PROFILE

Journal of
Materials Chemistry C

PAPER

Cite this: J. Mater. Chem. C, 2015, 3, 6686

Tunable near-infrared localized surface plasmon resonances of djurleite nanocrystals: effects of size, shape, surface-ligands and oxygen exposure time†

Dongxu Zhu,[a] Aiwei Tang,*[ab] Haihang Ye,[a] Miao Wang,[a] Chunhe Yang[a] and Feng Teng*[b]

Received 9th May 2015,
Accepted 17th May 2015

DOI: 10.1039/c5tc01310k

www.rsc.org/MaterialsC

Colloidal djurleite nanocrystals exhibit a well-defined and strong localized surface plasmon resonance absorption in the near-infrared region, which arises from the excess free holes in the valence band. The near-infrared localized surface plasmon resonance absorption wavelength of the as-obtained djurleite nanocrystals can be modulated by varying their size and shape, which are controlled through the variation of the reaction conditions during the synthesis. For a given size, the plasmonic behavior of the spherical nanocrystals exhibits an obvious surface-dependent shift due to the different electron-donating abilities of the surface ligands, which leads to the change of hole density. Moreover, the plasmonic band of the djurleite nanocrystals shifts to a shorter wavelength upon exposure to air for longer time, during which no crystal structure is altered, and this blue-shift may be attributed to the increasing density of copper vacancies. The experimental results of the near-infrared plasmonic behavior are in good agreement with the calculated results based on the Mie–Drude model.

1 Introduction

In the past few years, near-infrared (NIR) localized surface plasmon resonances (LSPRs) have been extensively studied for colloidal nonstoichiometric copper chalcogenide nanocrystals, such as $Cu_{2-x}S$ and $Cu_{2-x}Se$, which originate from excess holes in the valence band.[1–6] Since the NIR LSPR absorption of $Cu_{2-x}S$ nanocrystals could be slightly changed by varying the size and oxidation time in the pioneering work by Luther *et al.*,[1] much effort has been devoted to flexible manipulation of the plasmonic frequency by changing the size, crystal phase, composition and geometry of the copper chalcogenide nanocrystals.[7–16] For example, Zhao *et al.* found that the LSPR wavelength blue-shifted from $Cu_{1.97}S$ to $Cu_{1.8}S$ to CuS due to the increase of free carrier concentration.[7] Besides, Manna's group reported the tuning of the LSPR frequency of $Cu_{2-x}Se$ nanocrystals through an oxidation/reduction process.[10] These strategies open up new opportunities for copper chalcogenide nanocrystals with potential applications in chemiluminescence,[6] photothermal therapy,[17,18] imaging[19] and photovoltaics.[20]

It is well known that the nonstoichiometric $Cu_{2-x}S$ compounds have several polymorphs including Cu_2S (chalcocite), $Cu_{1.94}S$ (djurleite), $Cu_{1.8}S$ (digenite), $Cu_{1.75}S$ (anilite) and CuS (covellite), which are p-type semiconductors and exhibit a stoichiometry-dependent optical band gap.[4,7] Among them, djurleite is a copper sulfide mineral with a formula of $Cu_{31}S_{16}$ ($Cu_{1.94}S$), which possesses a cationic deficiency structure with a large unit cell containing 248 copper and 128 sulfur atoms.[21,22] Recent studies have demonstrated that the djurleite nanocrystals can serve as a seed catalyst to prepare heterostructure semiconductor nanocrystals, which have become a hot research topic in the family of copper sulfides.[23–26] In general, the chalcocite and djurleite phases have a similar crystal structure, and the Cu_2S has a thermodynamic instability which could transform into the copper-deficient $Cu_{2-x}S$ phases.[7] Due to the intrinsic copper-deficient characteristics, the LSPR behavior has been observed in the djurleite nanocrystals, but their absorption intensity is very weak.[7] To date, the LSPR properties of digenite and covellite nanocrystals have been studied in detail experimentally and theoretically.[4,9] However, the systematical investigation on the tuning of the LSPR frequency of djurleite nanocrystals has been rarely reported, especially in combination with experimental measurements and theoretical calculations, which is necessary

[a] Department of Chemistry, School of Science, Beijing JiaoTong University, Beijing 100044, China. E-mail: awtang@bjtu.edu.cn
[b] Key Laboratory of Luminescence and Optical Information, Ministry of Education, Beijing JiaoTong University, Beijing 100044, China. E-mail: fteng@bjtu.edu.cn

† Electronic supplementary information (ESI) available: Size distribution histogram, XRD patterns and typical XPS spectra of Sample A, representative TEM images and XRD patterns of Samples B and C, FTIR spectra of Samples A–C and TEM image and size distribution histogram of Sample C for studying the LSPR behavior upon exposure to air for different days. See DOI: 10.1039/c5tc01310k

to gain further insight into the plasmonic properties. In this paper, we have demonstrated the effects of the size, morphology, surface ligands and oxygen exposure time on the LSPR absorption of monoclinic djurleite nanocrystals, which were synthesized by using a simple heating-up approach. The LSPR behavior was sensitive to the functional groups of the surface ligands on the nanocrystals due to their different electron-donating abilities. Moreover, the exposure of the djurleite nanocrystals to air for different days caused an obvious blue-shift of the LSPR absorption band due to the increase of hole densities and copper vacancies. Moreover, the experimental results are in good agreement with the calculations based on the Drude model.

2 Experimental

Materials

Copper(II) acetylacetonate ($Cu(acac)_2$, 97%), oleic acid (OA, 85%) and oleylamine (OM, 80–90%) were purchased from Aladdin Reagent Company. 1-Octadecene (ODE, 90%) was purchased from Alfa Aesar. *n*-Dodecanethiol (DDT, 98%), ethanol, chloroform and tetrachloroethylene (TCE) were purchased from Sinopharm Chemical Reagent. All the above-mentioned chemicals were used as received without any purification.

Synthesis of djurleite nanocrystals

High-quality djurleite nanocrystals were synthesized based on our previous work.[27,28] For a typical synthesis of djurleite nanocrystals (Sample A), 5 mmol of $Cu(acac)_2$, 5 mL of DDT and 20 mL of OM were loaded in a 50 mL three-necked flask, and then the mixture was degassed using a N_2 flow under magnetic stirring for about 20 min. Afterwards, the mixture was heated slowly to 200 °C and kept for several hours. After the reaction was finished, the mixture was naturally cooled to room temperature by removing the heating mantle. The products were precipitated by adding excess ethanol and collected *via* centrifugation at 6000 rpm for 10 min. Next, the precipitation was dispersed in chloroform and centrifuged to remove the free surfactants and other insoluble species. This washing and centrifugation process was repeated three times, and the final products were dispersed in TCE or dried in a vacuum for further characterization. Moreover, other products were also synthesized by using OA and ODE to replace OM, while other reaction conditions were kept the same as Sample A, which were labelled as Sample B and Sample C, respectively.

Characterization

The crystal phase of the as-obtained products was characterized by using powder X-ray diffraction (XRD) patterns on a Bruker D8 Advance diffractometer using Cu Kα radiation (λ = 1.54056 Å). Transmission electron microscopy (TEM) images of the resultant products were taken using a JEM-1400 transmission electron microscope operating at an accelerating voltage of 100 kV. X-ray photoelectron spectroscopy (XPS) measurements were performed on a VG ESCALAB 220i-XL spectrometer using a 300 W Al Kα radiation source. The binding energies for all the different elements were calibrated with respect to the C 1s line at 284.8 eV from the contaminant carbon. The Fourier transform infrared (FTIR) spectrum was measured using a Varian Excalibur 3100 spectrometer. UV-vis-NIR absorption spectra were recorded using a Varian 5000 spectrophotometer. All of the measurements were performed at room temperature.

3 Results and discussion

In this reaction, the synthesis of djurleite nanocrystals involves the direct heating of $Cu(acac)_2$ in a mixed hot solvent of DDT and co-solvents such as ODE, OM and OA. In this case, $Cu(acac)_2$ and DDT are selected as the Cu source and the sulfur source. Furthermore, excess DDT also acts as a capping ligand. Other than ODE, OM and OA are also used as the capping agents to direct the growth of the as-obtained nanocrystals, except their role as the reaction media. Fig. 1a–e shows the TEM images of Sample A with different sizes and shapes, which can be tailored by varying the reaction time and temperature. As shown in Fig. 1a–c, the spherical djurleite nanocrystals have a good

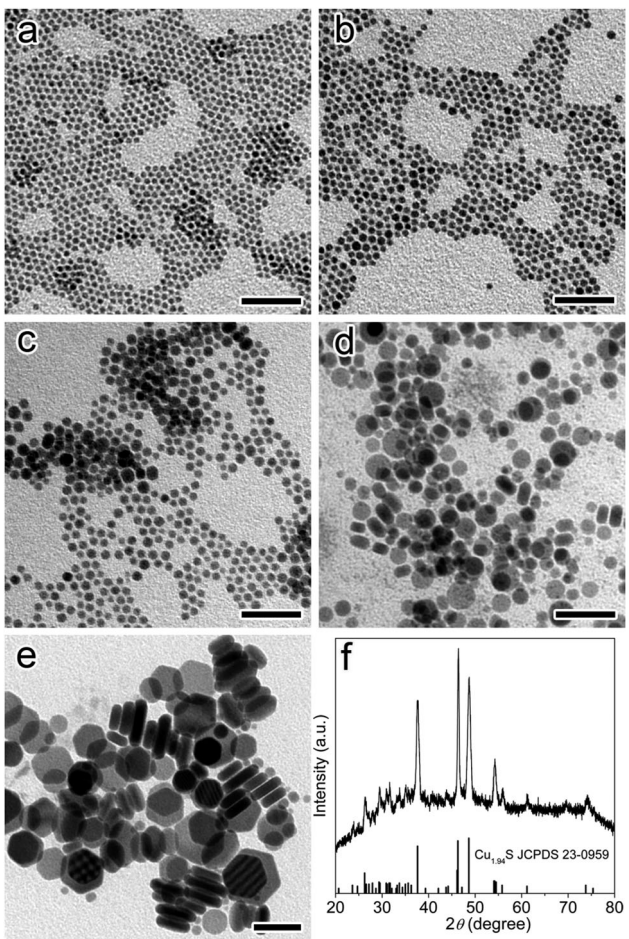

Fig. 1 TEM images of the djurleite nanocrystals with different sizes and shapes using OM as a co-surfactant: (a) 4.1 ± 0.3 nm, nanospheres; (b) 5.3 ± 0.5 nm, nanospheres; (c) 6.7 ± 0.6 nm, nanospheres; (d) 17.9 ± 3.5 nm, nanodisks; (e) 35.1 ± 9.1 nm, nanodisks and (f) XRD patterns of the as-obtained nanocrystals, which can be indexed as a monoclinic djurleite phase. All the scale bars are 50 nm.

monodispersity with a mean diameter of 4–7 nm. Fig. 1d and e depicts the TEM images of nanodisks, which can be confirmed by some particles with their faces perpendicular to the substrate to form the face-to-face assembly. The mean diameters (D) of the nanodisks are measured to be 17.9 ± 3.5 and 35.1 ± 9.1 nm, while their mean thickness (T) is kept in the range of 9–10 nm. The size distribution histograms of the products with different sizes are given in Fig. S1 of the ESI.† The typical XRD patterns of the djurleite nanodisks (D_{av} = 35.1 ± 9.1) are given in Fig. 1f, and all the diffraction peaks match well with the monoclinic djurleite ($Cu_{1.94}S$) phase, which confirms the formation of $Cu_{1.94}S$ nanocrystals. In consideration of the fact that the composition and the crystal phase of the resulting products may be varied by changing the reaction time and temperature, the XRD patterns of different-sized nanospheres and the nanodisks with a mean diameter of 17.9 ± 3.5 nm are given in Fig. S2 of the ESI,† and their crystal phases can be indexed as the monoclinic djurleite phase, which demonstrate that the crystal phase of the other samples remain unchanged. Moreover, XPS techniques have also been used to confirm the composition of the djurleite nanospheres with a mean size of 6.7 ± 0.6 nm and the nanodisks with a mean diameter of 17.9 ± 3.5 nm, and the high-resolution spectra of Cu 2p and S 2p are given in Fig. S3 of the ESI.† The absence of the satellite peak located between Cu $2p_{3/2}$ and Cu $2p_{1/2}$ indicates that the valence state of Cu should remain +1 in the nanospheres and nanodisks (Fig. S3a†).[23,27] The S 2p results can be fitted into the S $2p_{3/2}$ and S $2p_{1/2}$ peaks by using a 1.2 eV splitting (Fig. S3b†), and the S $2p_{3/2}$ peaks of the nanospheres and nanodisks are located at 161.9 eV and 161.4 eV, respectively, which can be assigned to the bound thiolate sulfur or the S ions coordinated to the metal ions.[23] The Cu/S atomic ratio of the nanodisks can be calculated to be 1.84 : 1, very close to the theoretical value of djurleite nanocrystals, which further confirms the formation of djurleite nanocrystals.

UV-vis-NIR spectroscopy has been employed to study the effects of size and shape on the LSPR behavior of djurleite nanocrystals.

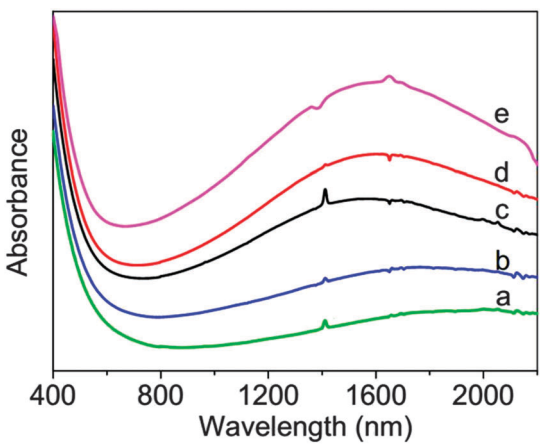

Fig. 2 NIR LSPR absorption spectra of djurleite nanocrystals with different sizes and shapes using OM as a co-solvent: (a) 4.1 ± 0.3 nm, nanospheres; (b) 5.3 ± 0.5 nm, nanospheres; (c) 6.7 ± 0.6 nm, nanospheres; (d) 17.9 ± 3.5 nm, nanodisks; (e) 35.1 ± 9.1, nm, nanodisks.

Fig. 2 shows the LSPR related absorption spectra of Sample A dispersed in TCE. An obvious decrease in the LSPR intensity and a blue-shift of the LSPR peak from 2030 nm to 1510 nm are observed with an increase in the diameter of Sample A with a spherical shape (Fig. 2). When the diameter is further increased from 6.7 nm to 17.9 nm while the shape is changed from nanospheres to nanodisks, a distinct red-shift of the LSPR absorption band is observed. In contrast, the plasmonic band of the djurleite nanoplates shifts from 1590 nm to 1510 nm with the aspect ratio (diameter-to-height) increasing from 2.1 (D = 17.9 ± 3.1 nm, T = 8.7 ± 0.7 nm) to 3.4 (D = 35.1 ± 9.1 nm, T = 10.4 ± 0.8 nm). According to work reported previously by Hsu *et al.*, the LSPR absorption band should be ascribed to the out-of-plane LSPR mode.[2,8] Herein, the variation result of the plasmonic peak *versus* the aspect ratio is consistent with the previous results in LSPR wavelengths for metal and $Cu_{2-x}S$ nanodisks.[8,29] For the bulk $Cu_{2-x}S$ films, the NIR absorbance arises from the excess holes in the valence band due to the copper deficiencies based on the previous report.[30] The carrier density can be calculated based on the Mie–Drude model, in which the relationship between the LSPR frequency (ω_{sp}) and the bulk plasma oscillation frequency (ω_p) can be expressed as follows:[9]

$$\omega_{sp} = \sqrt{\frac{{\omega_p}^2}{1 + \frac{1 - L_j}{L_j}\varepsilon_m} - \gamma^2} \quad (1)$$

where L_j is a shape-dependent geometrical factor with j = 1, 2, or 3 presenting three axes of the nanoparticle, ε_m represents the dielectric constant of the solvent and γ is the full-width half at maximum (fwhm) of the plasmon resonance band, which can be determined by fitting the NIR absorption band to a Gaussian function. Herein, for the solvent TCE, ε_m = 2.28. Based on the previous results, the geometrical factor L = 1/3 is available for the spherical particles.[31,32] As a result, the ω_p can be calculated to be 1.47–2.32 eV for different-sized nanospheres. Based on the bulk plasmon oscillation frequency (ω_p), the following equation is used to calculate the free carrier density (N_h):[1]

$$\omega_p = \sqrt{\frac{N_h e^2}{\varepsilon_0 m_h}} \quad (2)$$

where e is the electron charge, ε_0 is free space permittivity and m_h is the hole effective mass (approximated as 0.8 m_0, where m_0 is the electron mass). From the above equation, N_h is estimated to be 2.16–3.08 × 10^{21} cm^{-3} for the different-sized nanospheres (as shown in Table 1), which are of the same order of magnitude as the value of copper chalcogenide nanocrystals reported previously.[1,4] Based on the above information, the copper deficiencies of the djurleite nanospheres are calculated to be increased from 5.1% to 7.3%, which is responsible for the blue-shift of the LSPR absorption band. For the disk-shaped nanocrystals, the geometrical factor exhibits a strong dependence on the aspect ratio of the nanodisks, which can be approximated by considering them as the oblate spheroid structures.[33] Herein, the geometrical factor is calculated to be L = 0.38 and L = 0.48 for the different nanodisks with an aspect ratio of 2.1 and 3.4, respectively. Therefore, N_h can be estimated to be 2.55 × 10^{21} and 1.68 × 10^{21} cm^{-3}

Table 1 Summary of the shape, size of Sample A, and the corresponding important parameters of the theoretical calculations including LSPR frequency (ω_{sp}), the bulk plasma frequency (ω_p) and the free hole density (N_h)

Shape	Nanospheres			Nanodisks	
Size (nm)	4.1 ± 0.3	5.3 ± 0.5	6.7 ± 0.6	17.9 ± 3.5 8.7 ± 0.7	35.1 ± 9.1 10.4 ± 0.8
ω_{sp} (eV)	0.61	0.69	0.82	0.78	0.82
ω_p (eV)	1.47	2.16	2.29	2.08	1.64
N_h (10^{21} cm^{-3})	2.16	2.73	3.08	2.55	1.58

for the djurleite nanodisks with different aspect ratios (see Table 1), and the copper deficiencies are estimated to be 6% and 4%, respectively.

When OA and ODE were used to replace OM to act as the co-solvents, monoclinic djurleite nanocrystals were also successfully synthesized, and the XRD patterns are depicted in Fig. S4.† The TEM images of Sample B and Sample C shown in Fig. S5† indicate that both the products are spherical shape and have good monodispersity, and disk-like nanocrystals are observed in the TEM image of Sample B obtained at 240 min, which can be confirmed by some particles perpendicular to the substrate. Apart from the size and shape, the effect of the media dielectric constant on the LSPR frequency should be considered. In this work, two distinct surfactants OM and OA are incorporated into the syntheses of Samples A and B while non-coordinating ODE is used in the synthesis of Sample C. It is well known that the OM can coordinate to the surface *via* its amino functional group while OA can bind to the surface through its deprotonated carboxyl functional group.[34] Herein, it is predictable that OM and OA can act as co-surfactants to bind to the surface of Samples A and B in combination with DDT, but only DDT acts as a capping ligand in the synthesis of Sample C due to the non-coordinating ability of ODE. This plausible predication can be revealed using the FTIR results shown in Fig. S6,† in which the weak peak at 3300–3450 cm^{-1} due to the –NH_2 symmetric and asymmetric stretching vibration is observed in Sample A, while the peak at 1715–1730 cm^{-1} assigned to the free –COOH group is absent in Sample B.[3,35] Moreover, the absence of the band at 2577 cm^{-1} attributed to the S–H stretching vibration confirms the formation of the Cu–S bond.[23] Moreover, the effects of the dielectric constant of the three different surface ligands (OM, OA and DDT) on the LSPR behavior can be ruled out due to the similar refractive indices of these capping ligands (~1.46). Therefore, in this case, spherical djurleite nanocrystals with similar size have been selected to study the effects of surface ligands on the LSPR properties of the djurleite nanocrystals. Fig. 3 depicts the TEM images and the corresponding size distribution histograms of Samples A–C, and spherical nanocrystals are observed and the corresponding average diameter is 6.6–6.8 nm with a narrow size distribution less than 10%, which indicates that the as-obtained products have good monodispersity.

Fig. 4 displays the NIR LSPR absorption spectra of Samples A–C with similar average diameters. As shown in Fig. 4a, a little red-shift is observed in the LSPR wavelength of Samples A and B, but a notable red-shift of the LSPR wavelength is observed in Sample C. Based on the above discussion, this red-shift observed

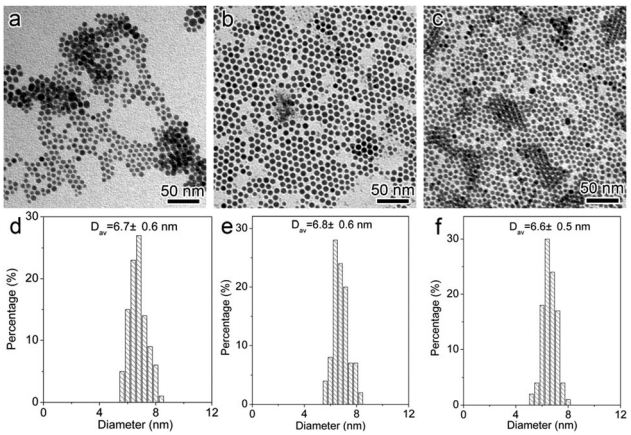

Fig. 3 TEM images and the corresponding size distribution histograms of (a, d) Sample A; (b, e) Sample B and (c, f) Sample C.

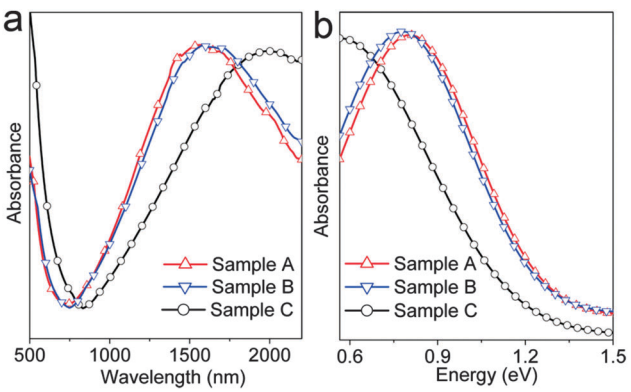

Fig. 4 (a) NIR LSPR absorption spectra of Samples A–C with similar diameters; (b) the LSPR absorption spectra on the energy scale, which are fitted based on the Gaussian function.

could not be explained only by the slight variation in the diameter of the nanocrystals, and the effects of the morphology and media dielectric constant should also be ruled out. Thus the difference of the electron-donating abilities of the three surface ligands may be responsible for the red-shift of the LSPR wavelength. As stated in the previous report, the thiol molecules often act as the electron rich species to donate electrons for the trapping sites at relatively low concentrations whilst they act as the hole traps at relatively high concentrations.[36] Thus, herein, excess thiolate on the surface of Sample C could trap free holes to reduce the hole concentrations. For Sample B, deprotonated OA is charged negatively which can donate electrons to decrease the hole density in Sample B. Moreover, the electron-denoting ability of OA is weaker than that of DDT, thus DDT can denote more electrons on the nanocrystal surface than OA, resulting in the decrease of hole density, which leads to a red-shift of the LSPR wavelength of Sample C as compared to that of Sample B. In the case of Sample A, the surfactant OM on the nanocrystal surface is uncharged; however, the lone pair of electrons of N atoms could also donate electrons, but their electron-donating ability is reduced greatly as compared to that of OA and DDT. Therefore, the LSPR wavelength of Samples B

Table 2 Summary of important parameters of the theoretical calculations

Sample	Diameter (nm)	ω_{sp} (eV)	ω_p (eV)	N_h (10^{21} cm^{-3})
Sample A	6.7 ± 0.6	0.82	2.29	3.08
Sample B	6.8 ± 0.6	0.78	2.21	2.87
Sample C	6.6 ± 0.5	0.58	2.07	2.52

and C shows a red-shift as compared to that of Sample A. To further demonstrate the deduction mentioned above, the Mie–Drude model has been employed to calculate N_h of Samples A–C based on eqn (1) and (2). The LSPR frequency (ω_{sp}) and line-width (γ) are determined by fitting the NIR absorption band on the energy scale to a Gaussian function, and the fitting result is given in Fig. 4b. Therefore, N_h is calculated to be 3.08×10^{21}, 2.87×10^{21} and 2.52×10^{21} cm^{-3} for Samples A, B and C, respectively. All the important parameters for the theoretical calculations are summarized in Table 2. The decreasing trend of N_h from the calculation results is in good agreement with the experimental results. All of the results further indicate that the electron-donating abilities of the capping ligands have a significant effect on the LSPR behavior of $Cu_{2-x}S$ nanocrystals.

Previous reports have demonstrated that the oxidation and reduction process is an effective method for controlling the composition and the crystal phase of $Cu_{2-x}S$, which leads to the variation of copper vacancies.[4,10] Moreover, the surface ligand OM has been proved to have a vital effect on the LSPR wavelength of CuS nanodisks after exposure to air in previous work.[9] Herein, we choose Sample C as the research objective to study the effects of the oxidation process on the LSPR behavior of the djurleite nanospheres, and the as-selected product exhibits a spherical shape with an average diameter of 9 nm (see Fig. S7†). Fig. 5 depicts the LSPR absorption spectra of Sample C upon exposure to oxygen (ambient air) for different days, and the insets show the corresponding LSPR frequency by fitting to a Gaussian function. An obvious blue-shift of the LSPR wavelength is observed after exposure to oxygen for different days as compared to that measured immediately on the day of synthesis. It should be noted that the blue-shift of the LSPR wavelength exhibits a decrease rate with the exposure time after keeping in air for 28 days, which indicates that the hole densities generated by the oxidation process reach saturation gradually. Based on the eqn (1) and (2), the N_h is calculated to be 2.21×10^{21} cm^{-3} for the fresh sample, and 2.74×10^{21} and 2.99×10^{21} cm^{-3} for the product exposure to oxygen for 28 and 55 days, respectively. These results indicate that the exposure to oxygen could induce more hole density. According to Liu's previous results, $Cu_{2-x}S$ nanocrystals could undergo phase or composition changes upon keeping in air for a few days.[4] However, no obvious crystal phase change is observed in our samples, as confirmed using the XRD results shown in Fig. 6. Nonetheless, a weak but non-ignorable diffraction peak 2θ = 51.5° appears in the XRD pattern of Sample C after keeping in air for 55 days, which may arise from copper oxides. Beyond that, all the other diffraction peaks of the products after 55 days match well with the monoclinic djurleite phase (JCPDS No. 23-0959). The XRD result indicates that the oxidation process just creates copper vacancies in the lattice without altering the crystal phase.[10] Therefore, the blue-shift of LSPR wavelength is not from the phase and composition transition. In addition, the TEM image of Sample C after exposure to air for 55 days is given in Fig. S8 of the ESI,† and quasi-spherical large particles appear with some aggregation, which may contribute to the blue-shift of the LSPR wavelength. Besides, the oxygen molecules can be easily adsorbed onto the surface of the nanocrystals by means of molecular electrostatic adhesion, and the adsorbed oxygen may act as an electron acceptor on the surface of the djurleite nanocrystals, which leads to the increase of the hole density *via* withdrawal of the electrons from the nanocrystals, thus the LSPR bands exhibit a blue-shift behavior.[9] To date, the contribution of the size effect and the oxygen adsorption has not been distinguished, and the further study is in progress. However, the exposure to air indeed leads to the increase of the hole density of the djurleite nanocrystals.

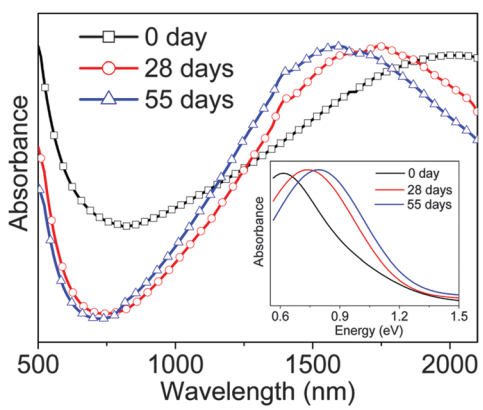

Fig. 5 NIR LSPR absorption spectra of Sample C upon exposure to oxygen (ambient air) for different days, and the inset shows the corresponding LSPR absorption spectra on the energy scale, which are fitted based on the Gaussian function.

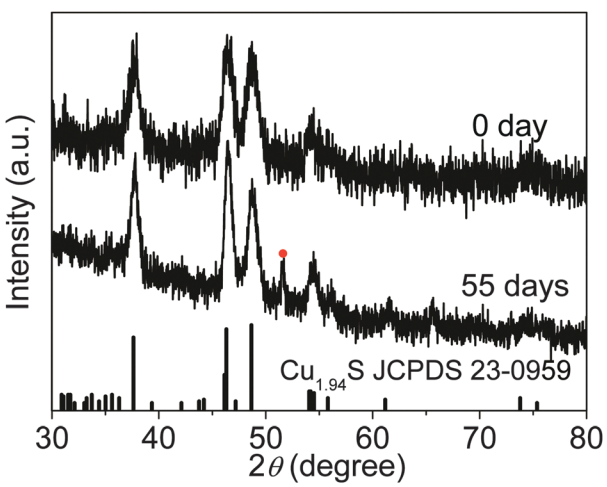

Fig. 6 XRD patterns of Sample C collected on the day of synthesis and after 55 days, and the red closed circle represents the peak from some oxides.

4 Conclusions

In summary, a simple heating-up colloidal method has been described for the production of djurleite nanocrystals with different sizes and shapes. The LSPR wavelength in the NIR region of the nanocrystals exhibits a size- and shape-dependent change, which is closely associated with the variation of the hole density. Moreover, the LSPR absorption band of the djurleite nanocrystals is sensitive to the surface ligands, which can be attributed to their different electron donating or accepting abilities. The LSPR behavior can also be tuned through the different oxygen exposure times, which generates more copper vacancies upon exposure to oxygen for more time. Calculations from the Mie–Drude model are in good agreement with the experimental results. These findings provide more pathways for tuning the LSPR bands of copper chalcogenides nanocrystals in the NIR region and offer more opportunities for their potential applications in IR imaging and spectroscopy.

Acknowledgements

This work was partly supported by the Fundamental Research Funds for the Central Universities (2014JBZ010), the National Natural Science Foundation of China (61108063), and the National Science Foundation for Distinguished Young Scholars of China (61125505). The author (M.W) appreciates the support from the Fundamental Research Funds for the Central Universities (S15JB00380).

Notes and references

1 J. M. Luther, P. K. Jaih, T. Ewers and A. P. Alivisatos, *Nat. Mater.*, 2011, **10**, 361.
2 S. W. Hsu, K. On and A. R. Tao, *J. Am. Chem. Soc.*, 2011, **133**, 19072.
3 X. Liu, X. L. Wang, B. Zhou, W. C. Law, A. N. Cartwright and M. T. Swihart, *Adv. Funct. Mater.*, 2013, **23**, 1256.
4 L. Liu, H. Zhong, Z. Bai, T. Zhang, W. Fu, L. Shi, H. Xie, L. Deng and B. Zou, *Chem. Mater.*, 2013, **25**, 4828.
5 X. Li, A. W. Tang, L. Guan, H. H. Ye, Y. B. Hou, G. Y. Dong, Z. P. Yang and F. Teng, *RSC Adv.*, 2014, **4**, 54547.
6 S. Q. Lie, D. M. Wang, M. X. Gao and C. Z. Huang, *Nanoscale*, 2014, **6**, 10289.
7 Y. X. Zhao, H. C. Pan, Y. B. Lou, X. F. Qiu, J. J. Zhu and C. Burda, *J. Am. Chem. Soc.*, 2009, **131**, 4253.
8 S. W. Hsu, W. Bryks and A. R. Tao, *Chem. Mater.*, 2012, **24**, 3765.
9 T. X. Wei, Y. F. Liu, W. J. Dong, Y. Zhang, C. Y. Huang, Y. Sun, X. Chen and N. Dai, *ACS Appl. Mater. Interfaces*, 2013, **5**, 10473.
10 D. Dorfs, T. Härtling, K. Miszta, N. C. Bigall, M. R. Kim, A. Genovese, A. Falqui, M. Povia and L. Manna, *J. Am. Chem. Soc.*, 2011, **133**, 11175.
11 O. A. Balitskii, M. Sytnyk, J. Stangl, D. Primetzhofer, H. Groiss and W. Heiss, *ACS Appl. Mater. Interfaces*, 2014, **6**, 17770.
12 H. H. Ye, A. W. Tang, C. H. Yang, K. Li, Y. B. Hou and F. Teng, *CrystEngComm*, 2014, **16**, 8684.
13 Y. Xie, A. Riedinger, M. Prato, A. Casu, A. Genovese, P. Guardia, S. Sottini, C. Sangregorio, K. Miszta, S. Ghosh, T. Pellegrino and L. Manna, *J. Am. Chem. Soc.*, 2013, **135**, 17630.
14 Y. Xie, L. Carbone, C. Nobile, V. Grillo, S. D'Agostino, F. D. Sala, C. Giannini, D. Altamura, C. Oelsner, C. Kryschi and P. D. Cozzol, *ACS Nano*, 2013, **7**, 7352.
15 I. Kriegel, C. Y. Jiang, J. Rodríguez-Fernández, R. D. Schaller, D. V. Talapin, E. da Como and J. Feldmann, *J. Am. Chem. Soc.*, 2012, **134**, 1583.
16 M. X. Liu, X. Z. Xue, C. Ghosh, X. Liu, Y. Liu, E. P. Furlani, M. T. Swihart and P. N. Prasad, *Chem. Mater.*, 2015, **27**, 2584.
17 C. M. Hessel, V. P. Pattani, M. Rasch, M. G. Panthani, B. Koo, J. W. Tunnell and B. A. Korgel, *Nano Lett.*, 2011, **11**, 2560.
18 Q. W. Tian, F. R. Jiang, R. J. Zou, Q. Liu, Z. G. Chen, M. F. Zhu, S. P. Yang, J. L. Wang, J. Wang and J. Q. Hu, *ACS Nano*, 2011, **5**, 9761.
19 X. Liu, C. Lee, W. C. Law, D. Zhu, M. Liu, M. Jeon, J. Kim, P. N. Prasad, C. Kim and M. T. Swihart, *Nano Lett.*, 2013, **13**, 4333.
20 Y. Zhao and C. Burda, *Energy Environ. Sci.*, 2012, **5**, 5564.
21 L. X. Yi, D. Wang and M. Y. Gao, *CrystEngComm*, 2012, **14**, 401.
22 T. Howard and J. Evans, *Science*, 1979, **203**, 356.
23 H. H. Ye, A. W. Tang, L. M. Huang, Y. Wang, C. H. Yang, Y. B. Hou, H. S. Peng, F. J. Zhang and F. Teng, *Langmuir*, 2013, **29**, 8728.
24 M. D. Regulacio, C. Ye, S. H. Lim, M. Bosman, L. Polavarapu, W. L. Koh, J. Zhang, Q. H. Xu and M. Y. Han, *J. Am. Chem. Soc.*, 2011, **133**, 2052.
25 S. K. Han, M. Gong, H. B. Yao, Z. M. Wang and S. H. Yu, *Angew. Chem., Int. Ed.*, 2012, **51**, 6365.
26 W. Han, L. X. Yi, N. Zhao, A. W. Tang, M. Y. Gao and Z. Y. Tang, *J. Am. Chem. Soc.*, 2008, **130**, 13152.
27 A. W. Tang, S. C. Qu, K. Li, Y. B. Hou, F. Teng, J. Cao, Y. S. Wang and Z. G. Wang, *Nanotechnology*, 2010, **21**, 285602.
28 A. W. Tang, F. Teng, Y. B. Hou, Y. S. Wang, F. R. Tan, S. C. Qu and Z. G. Wang, *Appl. Phys. Lett.*, 2010, **96**, 163112.
29 K. L. Kelly, E. Coronado, L. L. Zhao and G. C. Schatz, *J. Phys. Chem. B*, 2003, **107**, 668.
30 I. Grozdanov and M. Najdoski, *J. Solid State Chem.*, 1995, **114**, 469.
31 E. Ringe, J. Zhang, M. R. Langille, C. A. Mirkin, L. D. Marks and R. P. Van Duyne, *Nanotechnology*, 2012, **23**, 444005.
32 C. F. Bohren and D. R. Huffman, *Absorption and Scattering of Light by Small Particles*, Wiley, New York, 1983.
33 D. E. Charles, D. Aherne, M. Gara, D. M. Ledwith, Y. K. Gun'ko, J. M. Kelly, W. J. Blau and M. E. Brennan-Fournet, *ACS Nano*, 2010, **4**, 55.
34 S. Mourdikoudis and L. M. Liz-Marzán, *Chem. Mater.*, 2013, **25**, 1465.
35 M. Klokkenburg, J. Hilhorst and B. H. Erné, *Vib. Spectrosc.*, 2007, **43**, 243.
36 M. Green, *J. Mater. Chem.*, 2010, **20**, 5797.